

HRF-Net: Holistic Radiance Fields from Sparse Inputs

Phong Nguyen-Ha, Lam Huynh, Esa Rahtu, Jiri Matas, Janne Heikkilä

arXiv:2208.04717v1 [cs.CV] 9 Aug 2022

Abstract—We present HRF-Net, a novel view synthesis method based on holistic radiance fields that renders novel views using a set of sparse inputs. Recent generalizing view synthesis methods also leverage the radiance fields but the rendering speed is not real-time. There are existing methods that can train and render novel views efficiently but they can not generalize to unseen scenes. Our approach addresses the problem of real-time rendering for generalizing view synthesis and consists of two main stages: a holistic radiance fields predictor and a convolutional-based neural renderer. This architecture infers not only consistent scene geometry based on the implicit neural fields but also renders new views efficiently using a single GPU. We first train HRF-Net on multiple 3D scenes of the DTU dataset and the network can produce plausible novel views on unseen real and synthetic data using only photometric losses. Moreover, our method can leverage a denser set of reference images of a single scene to produce accurate novel views without relying on additional explicit representations and still maintains the high-speed rendering of the pre-trained model. Experimental results show that HRF-Net outperforms state-of-the-art generalizable neural rendering methods on various synthetic and real datasets.

Index Terms—novel view synthesis, neural rendering, volume-based rendering

I. INTRODUCTION

Novel view synthesis (NVS) is a long-standing task in computer vision and computer graphics that has applications in free-viewpoint video, telepresence, and mixed reality [1]. Novel view synthesis is a problem where visual content is captured from a set of sparse reference views and synthesized for an unseen target view. The problem is challenging since mapping between views depends on the 3D geometry of the scene and the camera poses between the views. Moreover, NVS requires not only propagation of information between the views, but also hallucination of details in the target view that are not visible in the reference image due to occlusions or limited field of view.

Early NVS methods produced target views by interpolating in ray [2] or pixel space [3]. They were followed by works that leveraged certain geometric constraints such as epipolar consistency [4] for depth-aware warping of the input views. These interpolation-based methods suffered from artifacts arising from occlusions and inaccurate geometry. Later works

Phong Nguyen-Ha, Lam Huynh and Janne Heikkilä are with the Center of Machine Vision and Signal Analysis, University of Oulu, Finland (e-mail: phong.nguyen@oulu.fi; lam.huynh@oulu.fi; janne.heikkila@oulu.fi).

Esa Rahtu is with the Faculty of Information Technology and Communication Sciences, Tampere University, Finland (e-mail: esa.rahtu@tuni.fi).

Jiri Matas is with the The Center for Machine Perception Department of Cybernetics, Czech Technical University, Prague (e-mail: matas@fel.cvut.cz).

tried to patch the artifacts by propagating depth values to similar pixels [5] or by soft 3D reconstruction [6]. However, these approaches cannot leverage depth information to refine the synthesized images or deal with the unavoidable issues of temporal inconsistency. Recently, Neural Radiance Fields (NeRF) made a significant impact on NVS research by implicitly representing the 3D structure of the scene and rendering photorealistic novel images. There are two main drawbacks of NeRF [7], which are: i) the requirement to train from scratch for every new scene separately and ii) slow rendering speed. Moreover, the per-scene optimization of NeRF is lengthy and requires densely captured images for each scene.

Recent approaches [8]–[13] address the former issue by training a generalized NeRF model to unseen scenes. The common strategy is to condition the NeRF renderer with features extracted from source images from a set of nearby views. Despite the generalization ability of these models to new scenes, the rendering speed is a bottleneck and they are unable to render novel views at an interactive rate. The reason of slow rendering is that these methods use implicit neural representation to render high-resolution images. Rendering such images requires querying millions of input 3D points to the NeRF model so real-time view synthesis is not possible. Also, there are NeRF-based methods that can render photorealistic novel images in real-time and requiring less than an hour for training. Despite such impressive results, these methods often rely on either differentiable explicit voxel representation [14]–[16] or a multi-resolution hash table [17] to store the neural scene representation. Therefore, those methods are not designed to render novel views of unseen scenes without performing the per-scene optimization.

In this work, we address the above issues by proposing a novel and efficient view synthesis pipeline that renders the entire view in a single forward pass during both training and testing. Inspired by the recently proposed works [10], [18], we first infer a low-resolution 3D volume from a few unstructured multi-view input images. MVSNeRF [10] decodes such volume using a Multi-Layer Perceptron (MLP) network to obtain volume densities and radiance values of the high-resolution target images which is slow to render. This motivates us to design a shallow, yet efficient attention-based network to holistically infer low-resolution radiance fields to overcome such a bottleneck. Through volume rendering, we obtain radiance features and depth maps at the novel viewpoints using the holistic radiance fields predictor. Instead of using the time-consuming coarse-to-fine rendering approach like [7], [8], we use the inferred depth maps to produce near-depth features of the target viewpoint and then fuse them with the radiance

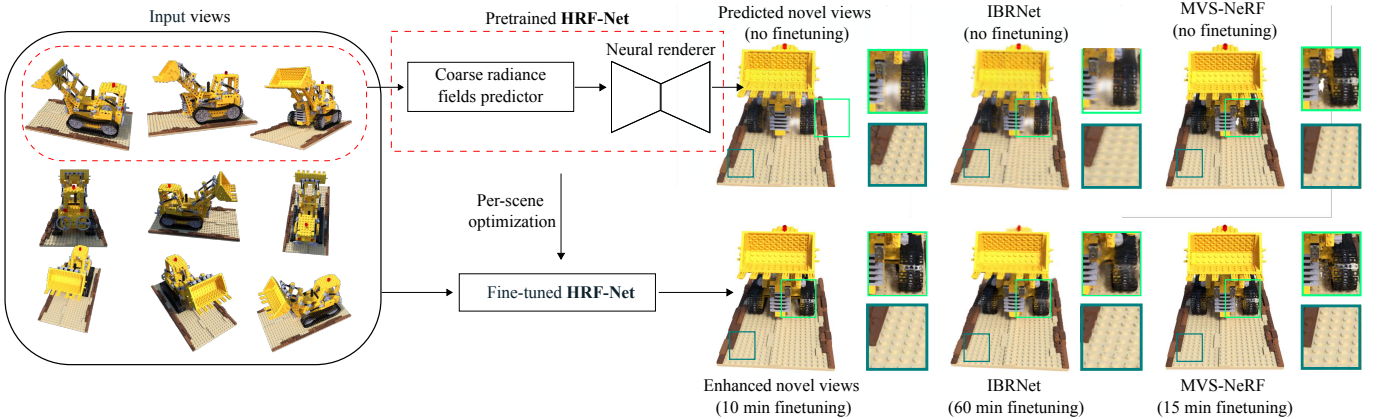


Fig. 1. HRF-Net is an efficient sparse view synthesis network that estimates coarse neural radiance fields of the target viewpoints at a low resolution and then renders the *entire* novel images efficiently via a convolutional-based neural renderer. Previous works [10], [21] do not possess such a renderer but rely on a deep fully connected network to estimate the high-resolution novel images pixel-by-pixel. Therefore, multiple forward passes are required to render pixels of novel views and this process often takes minutes to finish. In contrast, HRF-Net renders holistically the *entire* novel view more efficiently in a single forward pass and also requires less fine-tuning time than previous works to achieve state-of-the-art results.

features as inputs to a convolutional-based neural renderer. We then train both networks to produce high-resolution target images from low-resolution radiance features. Rendering the entire novel view also allows us to use perceptual loss [19] or adversarial training [20], which enhance the overall quality of the generated images. We also include a regularization loss to ensure that the predicted final images are consistent with the coarse estimated novel views from the holistic radiance field predictor.

We observe that our pretrained HRF-Net model renders plausible results on target poses which are close to the input viewpoints. However, the performance degrades when we extrapolate the targets further from the source views. Since our method depends on only a few sparsely captured reference images so it is challenging to render photorealistic targets that are beyond the field of view of the inputs. Previous works [10], [14]–[16] learn a hybrid implicit-explicit representation of radiance fields using a denser set of images that cover more views of a single scene. Using a similar approach, finetuning the pretrained HRF-Net model in 10–15 minutes produces state-of-the-art results compared to those produced by scene-specific approaches [13], [16]. Both pretrained and finetuned HRF-Net models do not require any explicit data structure but relying on a few selected reference views that are closest to the targets. As can be seen in Fig. 1, we also observe clear improvements in terms of visual quality between the novel views generated by the HRF-Net models and the other view synthesis methods [8], [10], [21]. Note that our method does not rely on depth supervision [18] to improve the quality of the synthesized images.

In summary, HRF-Net shows strong generalizability to render realistic images at novel viewpoints via a lightweight view synthesis network. If shortly further optimized with additional images, HRF-Net outperforms both recently proposed generalizable view synthesis methods [10], [13], [21] and per-scene optimized models [7], [16]. The main contributions of the work are:

- An efficient sparse view synthesis network that employs

a coarse radiance field predictor and a neural renderer to holistically predict novel images approximately two orders of magnitude faster than NeRF [7] and its variants [10], [13], [21].

- The proposed scene-specific model requires only 10–15 minutes of fine-tuning the pre-trained model using more images. In addition, HRF-Net does not require additional depth supervision.
- HRF-Net achieves state-of-the-art results in novel view synthesis on both real and synthetic datasets such as DTU [22], Synthetic-NeRF [7], Forward-Facing [23] and Tank&Temples [24].

Source code and neural network models will be made publicly available upon publication of the paper.

II. RELATED WORKS

In the following, we discuss different generalizable view synthesis methods using a set of sparse input views. For a more extensive review, we would like to refer to [25], [26].

Novel view synthesis. Early works based on deep learning often use a Plane Sweep Volume (PSV) [27]. Each input image is projected onto successive virtual planes of the target camera to form a PSV. Kalantari et al. [28] calculate the mean and standard deviation per plane of the PSV to estimate the disparity map and render the target view. Extreme View Synthesis (EVS) [29] builds upon DeepMVS [30] to estimate a depth probability volume for each input view that is then warped and fused into the target view. A similar coarse-to-fine scheme has been proposed by Nguyen et al. [18] but the method relies on depth supervision for view synthesis. Rather than estimating the depth maps of the source images, we train HRF-Net to predict the depth map at the target view via volumetric rendering. The inferred depth is then used to produce high-resolution appearance features which are later rendered as novel views.

Multi-layered representation. A significant number of works [31]–[34] on view synthesis represent the 3D scene by Multiple Plane Images (MPIs). Each MPI includes multiple RGB-

α planes, where each plane is related to a certain depth. The target view is generated by using alpha composition [35] in the back-to-front order. Zhou et al. [31] introduce a deep convolutional neural network to predict MPIs that reconstruct the target views for the stereo magnification task. Local Light Field Fusion (LLFF) [23] introduces a practical high-fidelity view synthesis model that blends neighboring MPIs to the target view. The input to the MPI-based methods is also PSVs. However, those PSVs are constructed for a fixed range of depth values. The proposed HRF-Net leverages coarse geometry and gathers near-surface features to enrich fine PSVs.

Voxel grid. Grid-based representations are similar to the MPI representation but are based on a dense uniform grid of voxels. This representation has been used as the basis for neural rendering techniques to model object appearance. Neural Volumes [36] is an approach for learning dynamic volumetric representations of multi-view data. The main limitation of grid-based methods is the required cubic memory footprint. The sparser the scene, the more voxels are empty, which wastes model capacity and limits output resolution. A recent work by Sun et al. [16] represents a 3D scene using low-resolution density and feature voxel grids for scene geometry and appearance. This method not only is fast to fit but produces high-quality novel views which are comparable with our fine-tuned HRF-Net model on a single scene. Instead of optimizing such voxel-grid representation [15], [16], [36], we propose using a memory-efficient architecture to encode multi-view input features into a single volume and infer the coarse geometry and appearance features of the entire target view in a single forward pass.

Pointclouds. Recent works [37]–[40] on view synthesis have also employed the point-based representation to model 3D scene appearance. A drawback of the point-based representation is that there might be holes between points after projection to the screen space. Aliev et al. [38] train a neural network to learn feature vectors that describe 3D points in a scene. These learned features are then projected onto the target view and fed to a rendering network to produce the final novel image. A recent work by Xu et al. [13] proposes a point-based radiance field representation that efficiently renders novel views within 15 minutes of training for each new scene. However, this method requires ground-truth depths to train a multi-view depth estimator network. In contrast, we only leverage photometric losses between the generated and ground-truth novel views to train our model. Experimental results show that HRF-Net can produce temporally consistent depths and novel views between multiple target viewpoints without relying on 3D supervision.

Neural radiance fields. The current state-of-the-art method Neural Radiance Fields (NeRF) by Mildenhall et al. [7] represents the plenoptic function by a multi-layer perceptron that can be queried using classical volume rendering to produce novel images. NeRF has to be evaluated at a large number of sample points along each camera ray. This makes rendering a full image with NeRF extremely slow. Despite the high quality of the synthesized novel images, NeRF also requires per-scene training. Recent volumetric approaches [8]–[13] address the generalization issue of NeRF by incorporating a latent

vector extracted from reference views. These methods show generalizability on selected testing scenes, but they share the slow rendering property of NeRF [7]. We propose a generalizable view synthesis network which speeds up volume rendering with convolutional layers to estimate the target views efficiently on a single GPU. The view synthesis results can also be enhanced by fine-tuning the obtained model on a single scene without using any additional components. Since HRF-Net is lightweight so it achieves faster rendering than NeRF and its variants.

III. PROPOSED METHOD

This section describes in detail the architecture of HRF-Net, which consists of two modules: a coarse radiance field predictor (Section III-A) that produces geometry and appearance of the scene at the lower resolution, and a convolutional-based neural renderer (Section III-B) that combines both coarse and fine features to produce the final target image at the original resolution. In addition, we discuss the loss functions to train the generalizable HRF-Net model and then finetune it on a single scene (Section III-C).

A. Coarse radiance field predictor

Our approach to inferring coarse radiance fields is orthogonal to many recent works [8], [10], [11], [21] on generalized view synthesis. Despite having impressive results, these methods are not able to render novel images in real-time. Since each pixel is rendered independently there are millions of query 3D points that are required to pass through the deep networks. This is an expensive process because the number of queries is much larger than the total amount of pixels rendered.

The main difference between HRF-Net and the above methods is that we infer radiance fields at the lower resolution so we can reduce the total amount of queried inputs and speed up the rendering process. By doing so, we can also obtain the geometry and appearance features of the *entire* target view in a single forward pass. Our method circumvents the slow rendering of NeRF [7] by avoiding splitting all queried 3D points into multiple chunks and rendering each chunk as a small image patch. Therefore, NeRF requires multiple forward passes to render multiple patches of the entire novel views. This also prevents NeRF and its variants [8], [10], [11], [21] to train their model using GAN or perceptual losses [20], [42] if stochastic pixels are generated during training. In contrast, we can train HRF-Net on these losses between the ground-truth images and the estimated novel views both at low and high resolution (see Section III-C).

Feature extraction. We first describe our pipeline (see Fig. 2) for estimating coarse radiance fields of the target viewpoints given a set of N unstructured input images $\{I_n\}_{n=1}^N$ and their poses. Each input image I_n is first fed to the Feature Pyramid Network [43] to extract $F_n^c \in \mathbb{R}^{H/4 \times W/4 \times C}$ and $F_n^f \in \mathbb{R}^{H \times W \times C/4}$ which are coarse and fine 2D image features, respectively. Note that, F_n^f has the same height H and width W as the original input so that we can later use them for the coarse-to-fine synthesis. At the coarse level, we do not know the scene geometry so we uniformly sample

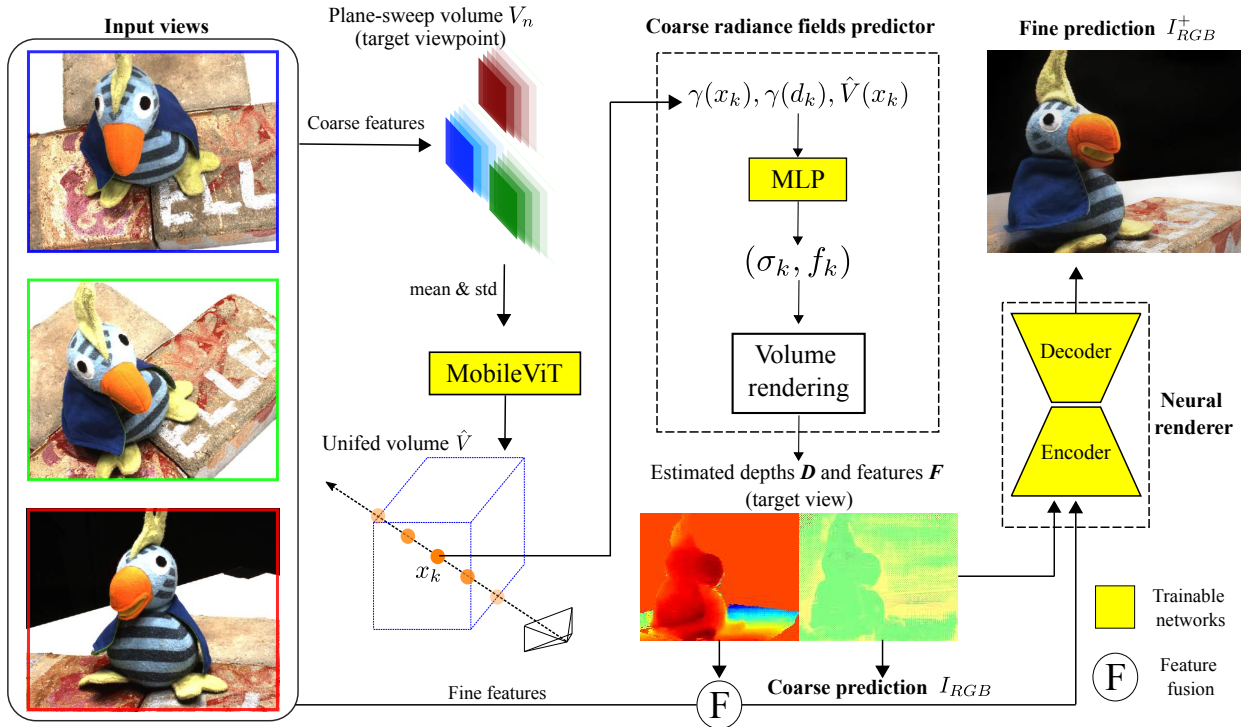


Fig. 2. Our proposed HRF-Net comprises several parts: (i) a memory-efficient MobileViT architecture [41] that fused multiple low-resolution plane-sweep volumes of the target viewpoint into a single unified volume \hat{V} , (ii) a coarse radiance fields predictor that estimates target depth and features in low resolution, and (iii) an auto-encoder network to render novel views at the original resolution. Our method is lightweight and can infer novel views in real-time.

several K virtual depth planes. Therefore, we leverage the coarse features of each input view to build a cost volume at the target viewpoint. This is achieved by warping 2D image features F_n^c into multiple hypothesis depth planes via bilinear sampling [10], [18]. The warped features are then concatenated to construct a per-view coarse volume $V_n \in \mathbb{R}^{H/4 \times W/4 \times K \times C}$.

Multi-view attention learning. Each volume V_n contains multiple-plane features of the target view so it requires a spatial reasoning architecture to aggregate those N volumes before the neural rendering step. Previous works [21], [44] use the vanilla Transformers which results in slow inference of the novel views due to the heavy computation of multi-head attention [45]. MVS-based methods [10], [18] opt on the mean and variance-based volumes that can later be processed by a 3D UNet to infer a unified scene encoding volume. However, a 3D Unet is limited due to the small receptive fields compared to attention-based architectures.

In this work, we try to combine the best of both approaches by using a single MobileViT block [41] which is a more memory-efficient variant of Transformers. We also compute the mean and variance between N volumes V_n and concatenate them as a statistic volume which is then passed to a single MobileViT block. This block learns the long-range dependencies via the multi-head attention [45] between the non-overlapping patches of those N volumes. We configure the input and output channels of the MobileViT block to produce a unified volume \hat{V} which has the same spatial dimension as V_n . By learning to attend to extracted multi-view features, the inferred volume encodes both scene geometry and appearance which can later be processed into volume densities and view-

dependent features for view synthesis.

Coarse radiance fields. Using the unified coarse volume \hat{V} , our method learns an MLP network M (see Fig. 3 (left)) to regress volume density $\sigma_k \in \mathbb{R}^1$ and appearance feature $f_k \in \mathbb{R}^C$ of a 3D point $x_k \in \mathbb{R}^3$ and its viewing direction $d_k \in \mathbb{R}^3$. More specifically, each 3D point x_k is the intersection between a ray shooting from the target camera and a virtual depth plane. We obtain the feature $\hat{V}(x_k)$ of sampled point x_k via trilinear interpolation [46]. The coarse radiance fields are then computed as follows:

$$(\sigma_k, f_k) = M(\gamma(x_k), \gamma(d_k), \hat{V}(x_k)) \quad (1)$$

where γ is the positional encoding function [7]. In this work, we estimate the per-point features f_k which can be used later for the neural renderer (described in Section III-B).

We design the model M as a shallow MLP network so that the training/inference speed can be faster than its NeRF counterparts. Instead of directly concatenating positional embedded $\gamma(x_k)$ and $\gamma(d_k)$ to image features, we use two different fully connected layers and project both embeddings into the latent space before combining them with the interpolated feature $\hat{V}(x_k)$. Adding those two extra layers does not increase the inference time but further improves the learning capacity of the model. In addition, our proposed architecture runs more efficiently than its NeRF counterparts since it inherits the massive speedup of the fully-fused connected layers [17] by treating the entire network as a single GPU kernel.

We also adopt the volume rendering approach of [7] to render novel depths and features via differentiable ray marching. Specifically, we can compute the per-ray feature F_r by

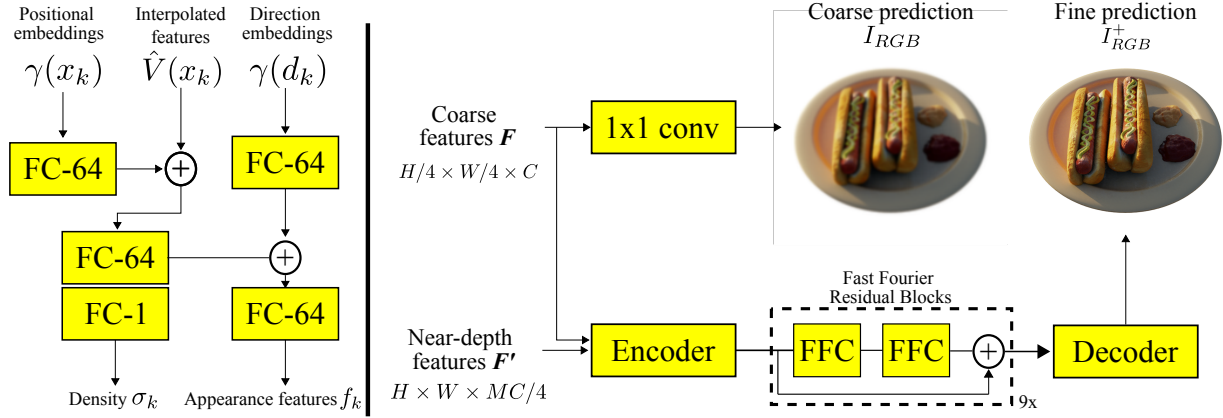


Fig. 3. Our proposed MLP model (left) uses several fully connected (FC) layers with 64 neurons each to estimate the coarse radiance fields of each sampled 3D point x_k . We also remove skip connections of the neural renderer (right) and add nine residual blocks which utilize Fast Fourier Convolution (FFC) [47] layers for generating the fine prediction I_{RGB}^+ of the novel views. A 1x1 convolution layer can also be added to estimate a coarse prediction I_{RGB} and regularize the training process. Finally, we use the dual discriminator of [20] to make sure that I_{RGB} and I_{RGB}^+ are visually consistent with each other.

accumulating f_k and σ_k of K sampled 3D points along a ray r as follows:

$$F_r = \sum_K \tau_k (1 - \exp(-\sigma_k \Delta_k)) f_k \quad (2)$$

$$\tau_k = \exp\left(-\sum_{t=1}^{k-1} \sigma_t \Delta_t\right) \quad (3)$$

where τ_i is the accumulated volume transmittance from ray origin to the point x_k and Δ_k is the distance between adjacent sampling points. Gathering all ray-features F_r of the target camera, we obtain the coarse feature maps $F \in \mathbb{R}^{H/4 \times W/4 \times C}$ of the novel view. We can also obtain the temporally consistent depth maps $D \in \mathbb{R}^{H/4 \times W/4}$ as a side-product of the volume rendering by calculating the weighted sum between estimated densities and depth values of x_k . Without learning to predict the novel depth maps at the original resolution, we up-sample the coarse depth maps D and use them to combine high-resolution input features F_n^f via a feature fusion step.

B. Neural renderer

Feature fusion. Once we get a coarse estimation of the scene geometry and appearance, we use an auto-encoder network to render the final target images. It is challenging to render such high resolution novel views using the coarse features F . Therefore, we leverage the depth plane resampling technique of [18] to obtain near-depth features F' which have the same spatial resolution as the target views. For each ray shooting from the target camera, we sample J points around the predicted depth value of the given ray. We then back-project those points into each input camera and obtain their corresponding features by bi-linear interpolating the extracted high-resolution input features F_n^f . Each pixel of $F' \in \mathbb{R}^{H \times W \times J \cdot C/4}$ is the weighted sum of the multi-view warped features and weights are defined as the inverse depths of the x_k at each input viewpoint. As the coarse radiance fields predictor gets better at predicting depth maps, so does the feature fusion method. Please refer to [18] for more details.

UNet renderer. To render the novel views at the high resolution, we up-sample the coarse feature F to match the spatial resolution of the original targets and then concatenate with F' before feeding to a fully convolutional UNet neural renderer which contains three up and down-sampling convolutional layers. Instead of using skip connections between the encoder and decoder, we employ several residual blocks with Fast Fourier Convolutions [47]–[49]. These blocks have the image-wide receptive field so they can effectively combine multi-scale features F and F' to render the high-resolution novel images I_{RGB}^+ . Without the skip connection between the encoder and decoder, the Unet model is also smaller and more efficient due to the reduced number of parameters.

C. Loss functions

We train both the coarse radiance field predictor and the auto-encoder network using a fine reconstruction loss \mathcal{L}_{fine} which is a combination of the L1 loss and perceptual [19] loss between I_{RGB}^+ and the ground-truth images. A 1×1 convolutional layer can also be added to transform coarse features F to low-resolution RGB color images I_{RGB} (see Fig. 3 (right)). This allows us to train HRF-Net using a coarse reconstruction L1 loss term \mathcal{L}_{coarse} between I_{RGB} and the down-scale ground-truths. This loss term also helps to regularize the coarse radiance fields learning without relying on the depth supervision [18]. To make sure that both I_{RGB} and I_{RGB}^+ are visually consistent with each other, we follow the dual discriminator set up of [20], add a hinge GAN [42] loss \mathcal{L}_{GAN} . Instead of discriminating over three-channel images, we perform the adversarial training using six-channel real and fake images. The fake image I_{RGB} is up-sampled before concatenating with I_{RGB}^+ . The ground-truth image is also down-sampled before concatenating with the original image. The total photometric loss to train HRF-Net is computed as: $\mathcal{L}_{total} = \mathcal{L}_{fine} + \mathcal{L}_{coarse} + \lambda \mathcal{L}_{GAN}$.

IV. EXPERIMENTS

In this section, we evaluate HRF-Net and compare the generated novel views to those produced by the state-of-the-art

TABLE I
QUANTITATIVE COMPARISON ON LARGE-SCALE DATASET OF SYNTHETIC AND REAL IMAGES.
METHODS WITH \dagger AND * SYMBOLS ARE OPTIMIZED PER SCENE FOR 15 AND 60 MINUTES RESPECTIVELY.

Methods	DTU [22]			Synthetic-NeRF [7]			Forward-Facing [23]			Tanks & Temples [24]		
	PSNR \uparrow	SSIM \uparrow	LPIPS \downarrow	PSNR \uparrow	SSIM \uparrow	LPIPS \downarrow	PSNR \uparrow	SSIM \uparrow	LPIPS \downarrow	PSNR \uparrow	SSIM \uparrow	LPIPS \downarrow
pixelNeRF [8]	19.31	0.78	0.38	7.39	0.65	0.41	11.24	0.48	0.67	-	-	-
MVSNeRF [10]	26.64	0.93	0.16	23.62	0.89	0.17	21.93	0.79	0.25	23.46	0.84	0.26
IBRNet [21]	26.04	0.92	0.19	22.44	0.87	0.19	21.79	0.78	0.28	21.70	0.81	0.29
PointNeRF [13]	23.89	0.87	0.2	-	-	-	-	-	-	-	-	-
HRF-Net	28.21	0.93	0.17	25.01	0.90	0.19	23.93	0.82	0.21	28.12	0.88	0.16
MVSNeRF \dagger [10]	28.50	0.94	0.17	27.05	0.93	0.16	25.45	0.87	0.19	28.39	0.89	0.15
IBRNet* [21]	31.35	0.95	0.13	25.62	0.94	0.11	24.88	0.86	0.18	26.12	0.85	0.21
PointNeRF \dagger [13]	30.12	0.95	0.11	30.71	0.96	0.08	-	-	-	29.61	0.95	0.08
DVGO \dagger [16]	31.49	0.96	0.10	31.95	0.96	0.05	-	-	-	-	-	-
HRF-Net\dagger	31.52	0.96	0.08	32.01	0.96	0.04	27.32	0.93	0.13	30.15	0.96	0.06

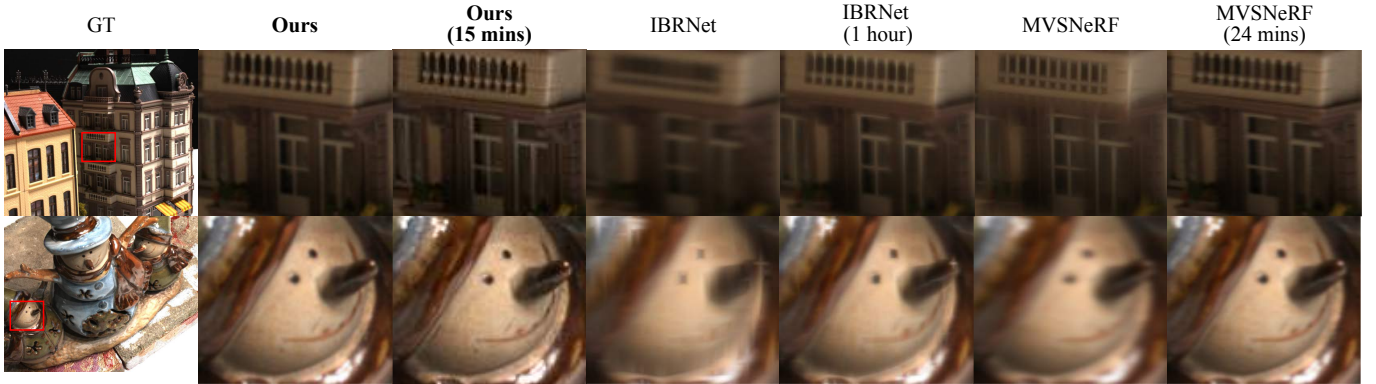


Fig. 4. Qualitative comparisons of view synthesis on the two testing sets of the DTU dataset [22]. Our HRF-Net can recover texture details and geometrical structures more accurately than other methods. Within 15 minutes of finetuning, HRF-Net outperforms state-of-the-art methods such as MVSNeRF [10] and IBRNet [21] which are required to more time to optimize using the same amount of data.

TABLE II
SPEED COMPARISONS OF RENDERING A 800x800 NOVEL IMAGE
BETWEEN HRF-NET AND OTHER VIEW SYNTHESIS METHODS.

Methods	IBRNet [21]	MVSNeRF [10]	PointNeRF [13]	DVGO [16]	Ours
Time (seconds)	29	15	10	0.64	0.2

methods.

A. Implementations

Model details. The models were trained with the Adam optimizer using a 0.004 learning rate for the discriminator, 0.001 for both the coarse radiance field predictor and the neural renderer with the momentum parameters (0, 0.9). $\lambda = 0.5$, $C = 64$, $K = 64$, $J = 4$, $N = 3$, $W = 640$, $H = 512$ and the MobileViT block had 4 attention heads for fast inference. We used the Pytorch extension of the tiny-cuda-nn [50] library for the fully-fused connected layers. The other modules of HRF-Net are implemented using native PyTorch. We first trained the model from scratch on multiple scenes in 16 hours using four V100 GPUs with a batch size of 16. A 10-15 min fine-tuning on a V100 GPU is required to achieve state-of-the-art results for per-scene optimization. After fine-tuning, we tested HRF-Net on a consumer-grade RTX 2080TI GPU.

View selection. We follow the view selection method of [51] to choose the top 10 closest source images to each target image. During training, we randomly select N source images among the 10 closest views as inputs to our method. At each training step, N is uniformly sampled between 3-5.

B. Experiments

Datasets. We train HRF-Net on the DTU [22] dataset to learn a generalizable network. DTU is an MVS dataset consisting of more than 100 scenes scanned in 7 different lighting conditions at 49 positions. From 49 camera poses, we selected 10 as targets for view synthesis and used the rest for source image selection. We evaluate the performance of our pretrained model using the testing set of the DTU dataset. To further compare HRF-Net with state-of-the-art methods, we test it on the Synthetic-NeRF [7], Forward-Facing [23], and Tanks & Temples [24] datasets, which have different scenes and view distributions from our training set. Each scene includes 12 to 62 images and 1/8 of these images are held out for testing.

Baselines. In this evaluation, we compare HRF-Net to both generalizable view synthesis and pure per-scene optimized methods. The former approaches [8], [10], [21] predict new views with and without per-scene optimization. We use their provided pre-trained models and then finetune for each testing scene for fair comparisons. Furthermore, we compare our

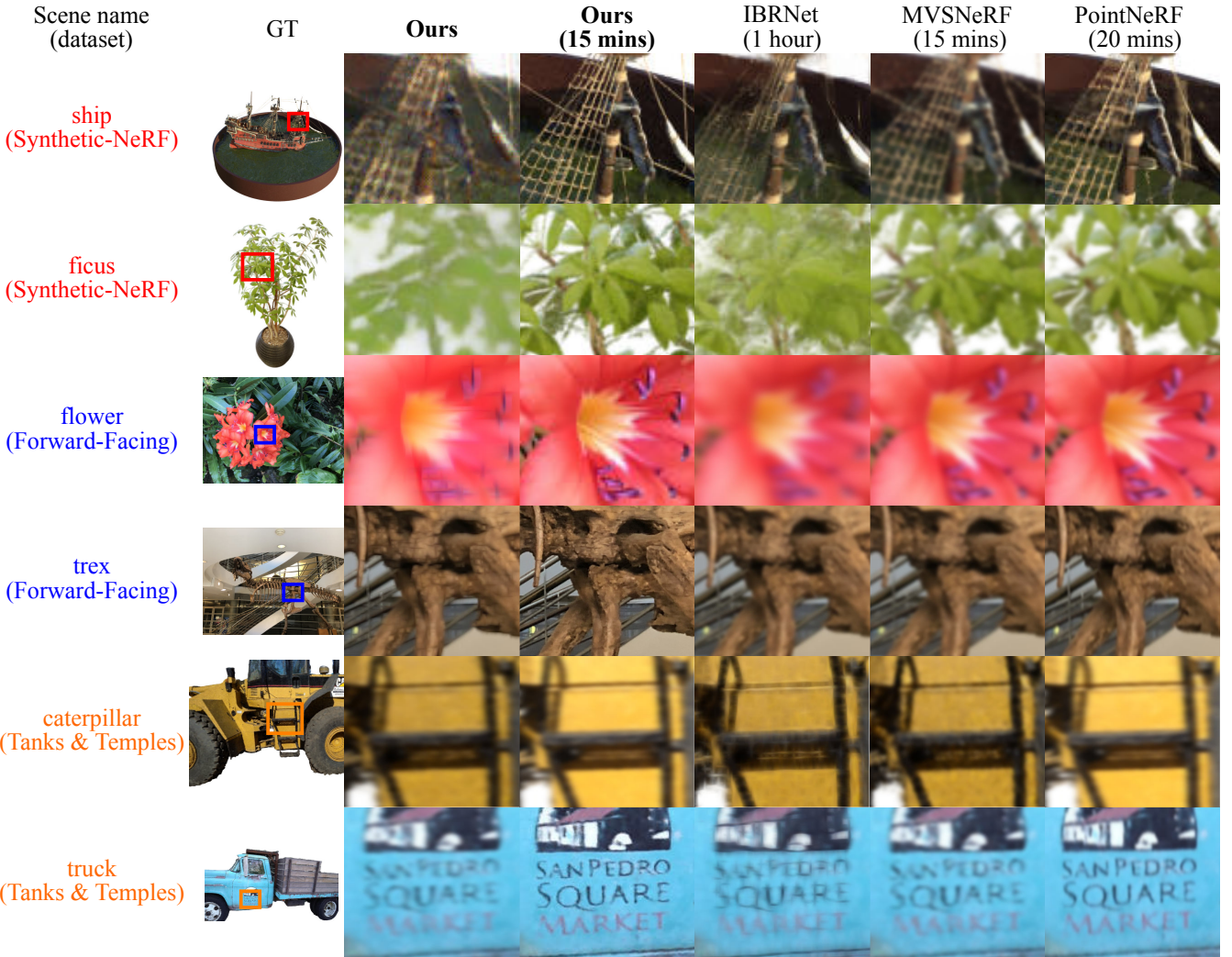


Fig. 5. Qualitative comparisons between HRF-Net and state-of-the-art methods on unseen data. Each row shows estimated novel views of three different datasets: Synthetic-NeRF [7], Forward-Facing [23], and Tanks & Temples [24]. Without any finetuning, our pre-trained model can produce plausible results on unseen data and the results are vastly improved after optimizing on a single scene. In general, our method produces more accurate textures and thin structure objects than those produced by other baselines.

method with the recent scene-specific synthesis methods such as PointNeRF [13] and DVGO [16]. We use their public code to train scene-specific models and compare the generated novel views with those produced by our method both qualitatively and quantitatively.

Metrics. We report the PSNR, SSIM, and perceptual similarity (LPIPS) [52] for HRF-Net and other state-of-the-art methods. We summarize the quantitative and qualitative results in Table I, Fig. 4, and Fig. 5 using samples from four different datasets [7], [22]–[24]. Please see the supplementary video for more qualitative results.

Testing on the seen dataset. We first evaluate HRF-Net on the testing set of the DTU dataset. Since our methods are trained on the training set of the same dataset, we observe both pretrained HRF-Net and per-scene optimized HRF-Net[†] can reconstruct accurate novel views on the unseen testing scenes as can be seen in the second and third column of Fig. 4. Moreover, they outperform other state-of-the-art methods both quantitatively and qualitatively. The direct inference network

of IBRNet [21] and MVSNeRF [10] are not able to produce faithful textures of the windows and the reflection at the tip of the nose of the toy character. Both baselines tend to predict blurry results and fail to retrieve fine details as can be seen in the zoomed insets of Fig. 4. Since these methods predict each pixel of the high-resolution novel views from a low-resolution feature volume, their MLP network have to solve two difficult tasks which are image synthesis and super-resolution. Instead, we tackle these two tasks by two different networks: one to estimate coarse radiance features and another to refine them using the adversarial training and a convolution-based neural renderer. As can be seen in Fig. 4, the rendering results of IBRNet* and MVSNeRF[†] are sharper if both models are optimized for each testing scene. Note that, they both required approximately 24 minutes up to 1 hour to achieve sharp results but still achieve less accurate novel views than ours which are fine-tuned in 15 minutes for all testing scenes.

Testing on the unseen dataset. To further test the generalizability of our approach on unseen data, we conduct experi-

ments on three synthetic and real datasets. As can be seen in the second column of Fig. 5, HRF-Net can produce plausible results on all testing novel views which are very different from the training DTU images. Despite not seeing those testing images, the HRF-Net model shows competitive results with a variant of MVSNeRF[†] which is trained for the same amount of time as ours. Given almost one hour of finetuning, IBRNet* improves its results significantly but is still not able to estimate as accurate novel views as ours. Optimizing for a quarter of an hour, HRF-Net[†] produces cleaner and more photo-realistic novel views than those produced by MVSNeRF[†] and IBRNet* on these unseen synthetic and real datasets. Despite being trained on the testing scenes, both baseline methods are not able to render such fine details because they only use a L2 color loss between stochastic rendered and ground-truth pixels. On the ship scene of the Synthetic-NeRF dataset, our optimized HRF-Net[†] model can render the thin structure of the sky-sail which is not visible on the generated novel views of other methods. High-frequency details can be seen in the generated images of our method on the real flower and trex scenes of the Forward-Facing dataset. Moreover, we can also observe that HRF-Net[†] estimates clearer text on the door of the truck scene in the second example of the Tank&Temples dataset. Although our pretrained HRF-Net model is not able to retrieve such fine details, the rendering results can be vastly improved thanks to the hinge GAN loss \mathcal{L}_{GAN} that we applied during training. Note that, it is not straightforward for other baselines to perform adversarial training due to the limited resolution of the generated images. This is not a problem with our methods because we can efficiently render the entire novel views without worrying about the out-of-memory issue which is unavoidable for other baselines.

We also compare our methods with state-of-the-art scene-specific view synthesis PointNeRF [13] models. Since this method is not designed for generalizable view synthesis, it performs worse than HRF-Net. However, we observe a significant gain in performance of the fine-tuned PointNeRF[†] model across testing data. As can be seen in the last column of Fig. 5, PointNeRF[†] can render fine details but the generated novel views are still not as accurate as ours in all testing scenes. In the challenging ficus scene of the Synthetic-NeRF dataset, our method can render the leaves sharper than PointNeRF[†], which renders high-resolution novel views from a point-cloud where the feature of each point is interpolated from low-resolution image features. Despite using a memory-expensive point-cloud representation, PointNeRF[†] is still not able to render high-quality details of the novel views, especially when we zoom closely into the content of the generated images.

Improving PointNeRF [13]. To further demonstrate the effectiveness of our method, we apply our proposed convolution-based neural renderer to the PointNeRF architecture. We have made some changes to improve the results: i) we modify the output resolution of PointNeRF model to match the spatial size of the input volume feature and ii) we then perform the adversarial training on the generated novel views and ground-truth images. After training, we observe that the rendering results of the improved pointNeRF are competitive with HRF-Net[†] but the rendering speed of is still approximately 10 times slower

TABLE III
HRF-NET ARCHITECTURE ABLATION STUDY. RECONSTRUCTION ACCURACY OF VIEW SYNTHESIS ON THE FORWARD-FACING SCENES [22].

Random rays	Holistic	\mathcal{L}_{coarse}	\mathcal{L}_{GAN}	PSNR↑	SSIM↑	LPIPS↓
✓				19.15	0.82	0.34
	✓			20.59	0.76	0.30
	✓	✓		22.19	0.80	0.25
	✓	✓	✓	23.93	0.82	0.21

than our approach. This further highlights the usefulness of our proposed MLP architecture and the neural renderer.

Rendering speed. In this section, we compare the rendering speed between HRF-Net and other view synthesis methods. In general, our method not only produces better novel views but also renders them faster than previous works. IBRNet takes almost 30 seconds to render a single novel image because the method uses the time-consuming Transformer architecture for multi-view aggregation and it also inherits the slow rendering of NeRF. Both MVSNeRF and PointNeRF improve the speed by rendering the novel views directly from their hybrid implicit-explicit volume representations. However, both methods are still slow and not able to render novel views in a real-time manner. Our finetuned HRF-Net[†] model also shows competitive results with a recently proposed DVGO [16] method. This method proposes using coarse and fine neural radiance volumes and achieves not only quick convergence but also fast rendering speed (0.64 second/image). As can be seen in the Table II, HRF-Net can render novel views much faster (0.2 second/image). We found that rendering the entire novel views using the proposed fully-fused MLP and convolution-based neural renderer is faster than sequentially rendering individual pixels using a deep MLP model of NeRF and its variants.

V. ABLATION STUDY

A. Architecture design

Table III and Fig. 6 summarize the quantitative and qualitative results of HRF-Net on different architectural choices using the test set of the Forward-Facing dataset [24]. We first define a "Random rays" variant of HRF-Net that estimates stochastic sampled pixels [10], [21] of the high-resolution novel views during training. Independently rendering each pixel leads to visible artifacts and blurriness of the predicted novel views. The rendering results are better if we holistically estimate of the novel views using a convolution-based neural renderer. However, this model does not produce plausible target views as they still contain incorrect geometry and poorly rendered specular areas. By regularizing our model with a coarse reconstruction loss \mathcal{L}_{coarse} , we address the above issues and observe vastly improved novel views. Finally, we found that adding a hinge GAN loss \mathcal{L}_{GAN} and the dual discriminator of [20] helps us to achieve state-of-the-art results as can be seen in the last column of Fig. 6. We provide more comparison results in the supplementary videos.

B. Number of input views

In Table IV, we evaluate the performance of our method with an increasing number of source images using the Tanks

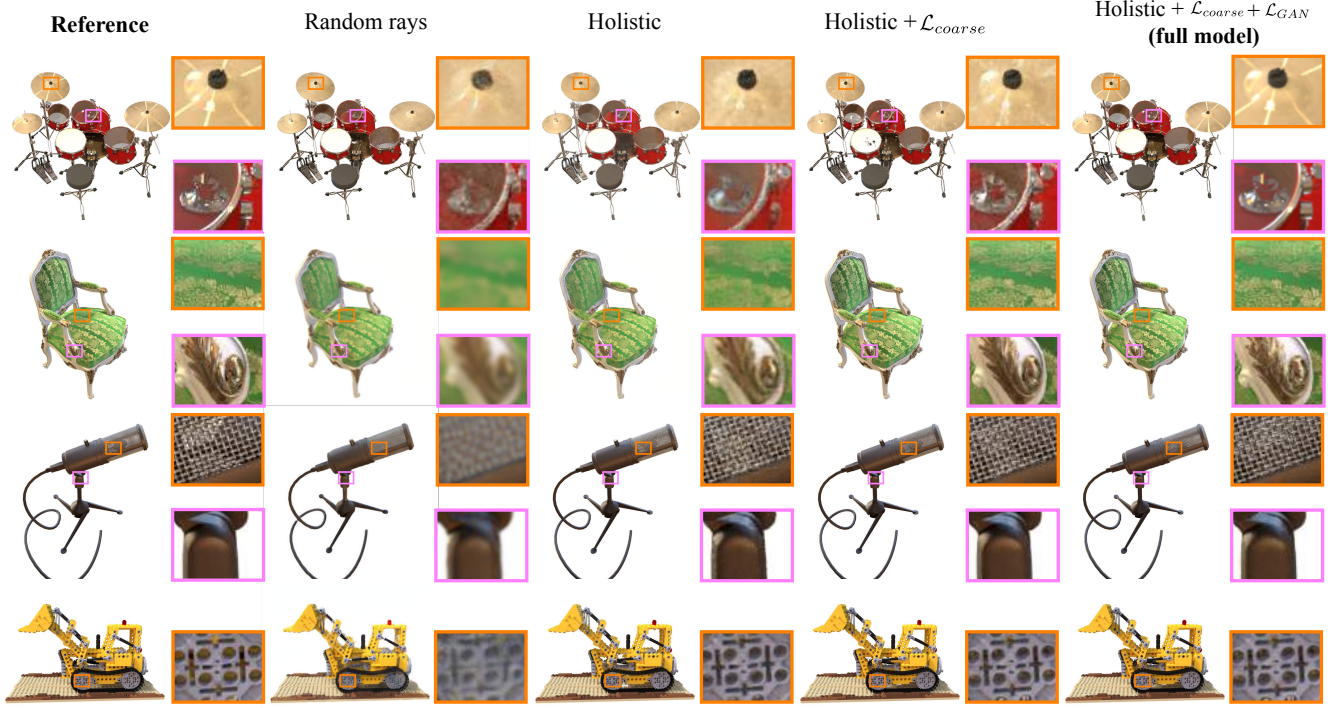


Fig. 6. Qualitative ablation study. Comparison of ground-truth with predicted novel views by HRF-Net with random and holistic training, with coarse reconstruction loss \mathcal{L}_{coarse} and the full model with enabled adversarial loss \mathcal{L}_{GAN} . The full model not only predicts novel views more accurate than other baselines but also render them efficiently thanks to holistic training. Without using \mathcal{L}_{GAN} , we observe less realistic novel images compared to the ground-truths.

TABLE IV

THE IMPACT OF THE NUMBER OF REFERENCE IMAGES, MEASURED IN TERMS OF RECONSTRUCTION ACCURACY ON THE TANK&TEMPLES [24].

	# of reference images						
	4	5	6	7	8	9	10
LPIPS↓	0.267	0.203	0.185	0.160	0.168	0.171	0.175
SSIM↑	0.796	0.825	0.871	0.892	0.890	0.890	0.887

and Temples [24] dataset. We report both SSIM and LPIPS metrics with the number of source images up to 10. We observe that HRF-Net performs the best with 7 input views and then the results get worse.

VI. CONCLUSION

We presented HRF-Net, a new method to address the challenging problem of novel view synthesis from a sparse and unstructured set of input images. Due to its coarse neural radiance field predictor and a convolution-based neural renderer, HRF-Net can produce all pixels of the target view in a real-time manner. Moreover, it enables highly efficient per-scene optimization that takes only 10-15 minutes, leading to rendering quality comparable to and even surpassing recent state-of-the-art methods which require several hours of training.

REFERENCES

- [1] N. K. Shukla, S. Sengupta, and M. Chakraborty, “Intermediate view synthesis in wide-baseline stereoscopic video for immersive telepresence,” in *The 2nd European Workshop on the Integration of Knowledge*, Semantics and Digital Media Technology, 2005. EWIMT 2005. (Ref. No. 2005/11099), 2005, pp. 83–88.
- [2] M. Levoy and P. Hanrahan, “Light field rendering,” in *Proceedings of the 23rd Annual Conference on Computer Graphics and Interactive Techniques*, ser. SIGGRAPH ’96. New York, NY, USA: Association for Computing Machinery, 1996, p. 31–42. [Online]. Available: <https://doi.org/10.1145/237170.237199>
- [3] S. E. Chen and L. Williams, “View interpolation for image synthesis,” in *Proceedings of the 20th Annual Conference on Computer Graphics and Interactive Techniques*, ser. SIGGRAPH ’93. New York, NY, USA: Association for Computing Machinery, 1993, p. 279–288. [Online]. Available: <https://doi.org/10.1145/166117.166153>
- [4] C. Buehler, M. Bosse, L. McMillan, S. Gortler, and M. Cohen, “Unstructured lumigraph rendering,” in *Proceedings of the 28th Annual Conference on Computer Graphics and Interactive Techniques*, ser. SIGGRAPH ’01. New York, NY, USA: Association for Computing Machinery, 2001, p. 425–432. [Online]. Available: <https://doi.org/10.1145/383259.383309>
- [5] G. Chaurasia, S. Duchene, O. Sorkine-Hornung, and G. Drettakis, “Depth synthesis and local warps for plausible image-based navigation,” *ACM Trans. Graph.*, vol. 32, no. 3, Jul. 2013. [Online]. Available: <https://doi.org/10.1145/2487228.2487238>
- [6] E. Penner and L. Zhang, “Soft 3d reconstruction for view synthesis,” *ACM Trans. Graph.*, vol. 36, no. 6, Nov. 2017. [Online]. Available: <https://doi.org/10.1145/3130800.3130855>
- [7] B. Mildenhall, P. P. Srinivasan, M. Tancik, J. T. Barron, R. Ramamoorthi, and R. Ng, “Nerf: Representing scenes as neural radiance fields for view synthesis,” in *ECCV*, 2020.
- [8] A. Yu, V. Ye, M. Tancik, and A. Kanazawa, “pixelNeRF: Neural radiance fields from one or few images,” in *CVPR*, 2021.
- [9] A. Trevithick and B. Yang, “Grf: Learning a general radiance field for 3d representation and rendering,” in *Proceedings of the IEEE/CVF International Conference on Computer Vision*, 2021, pp. 15 182–15 192.
- [10] A. Chen, Z. Xu, F. Zhao, X. Zhang, F. Xiang, J. Yu, and H. Su, “Mvsnerf: Fast generalizable radiance field reconstruction from multi-view stereo,” in *Proceedings of the IEEE/CVF International Conference on Computer Vision*, 2021, pp. 14 124–14 133.
- [11] J. Chibane, A. Bansal, V. Lazova, and G. Pons-Moll, “Stereo radiance fields (srdf): Learning view synthesis for sparse views of novel scenes,”

- in *Proceedings of the IEEE/CVF Conference on Computer Vision and Pattern Recognition*, 2021, pp. 7911–7920.
- [12] M. M. Johari, Y. Lepoittevin, and F. Fleuret, “Geonerf: Generalizing nerf with geometry priors,” *arXiv preprint arXiv:2111.13539*, 2021.
- [13] Q. Xu, Z. Xu, J. Philip, S. Bi, Z. Shu, K. Sunkavalli, and U. Neumann, “Point-nerf: Point-based neural radiance fields,” *arXiv preprint arXiv:2201.08845*, 2022.
- [14] L. Liu, J. Gu, K. Z. Lin, T.-S. Chua, and C. Theobalt, “Neural sparse voxel fields,” *NeurIPS*, 2020.
- [15] Sara Fridovich-Keil and Alex Yu, M. Tancik, Q. Chen, B. Recht, and A. Kanazawa, “Plenoxels: Radiance fields without neural networks,” in *CVPR*, 2022.
- [16] C. Sun, M. Sun, and H.-T. Chen, “Direct voxel grid optimization: Super-fast convergence for radiance fields reconstruction,” *arXiv preprint arXiv:2111.11215*, 2021.
- [17] T. Müller, A. Evans, C. Schied, and A. Keller, “Instant neural graphics primitives with a multiresolution hash encoding,” *arXiv:2201.05989*, Jan. 2022.
- [18] P. Nguyen-Ha, A. Karnewar, L. Huynh, E. Rahtu, and J. Heikkila, “Rgbd-net: Predicting color and depth images for novel views synthesis,” in *Proceedings of the International Conference on 3D Vision*, 2021.
- [19] Q. Chen and V. Koltun, “Photographic image synthesis with cascaded refinement networks,” in *IEEE International Conference on Computer Vision, ICCV 2017, Venice, Italy, October 22-29, 2017*. IEEE Computer Society, 2017, pp. 1520–1529. [Online]. Available: <https://doi.org/10.1109/ICCV.2017.168>
- [20] E. R. Chan, C. Z. Lin, M. A. Chan, K. Nagano, B. Pan, S. D. Mello, O. Gallo, L. Guibas, J. Tremblay, S. Khamis, T. Karras, and G. Wetzstein, “Efficient geometry-aware 3D generative adversarial networks,” in *arXiv*, 2021.
- [21] Q. Wang, Z. Wang, K. Genova, P. P. Srinivasan, H. Zhou, J. T. Barron, R. Martin-Brualla, N. Snavely, and T. Funkhouser, “Ibrnet: Learning multi-view image-based rendering,” in *Proceedings of the IEEE/CVF Conference on Computer Vision and Pattern Recognition*, 2021, pp. 4690–4699.
- [22] H. Aanaes, R. R. Jensen, G. Vogiatzis, E. Tola, and A. B. Dahl, “Large-scale data for multiple-view stereopsis,” *Int. J. Comput. Vision*, vol. 120, no. 2, p. 153–168, Nov. 2016. [Online]. Available: <https://doi.org/10.1007/s11263-016-0902-9>
- [23] B. Mildenhall, P. Srinivasan, R. Ortiz-Cayon, N. K. Kalantari, R. Ramamoorthi, R. Ng, and A. Kar, “Local light field fusion: Practical view synthesis with prescriptive sampling guidelines,” *ACM Transactions on Graphics (TOG)*, 2019.
- [24] A. Knapsitsch, J. Park, Q.-Y. Zhou, and V. Koltun, “Tanks and temples: Benchmarking large-scale scene reconstruction,” *ACM Transactions on Graphics*, vol. 36, no. 4, 2017.
- [25] A. Tewari, O. Fried, J. Thies, V. Sitzmann, S. Lombardi, K. Sunkavalli, R. Martin-Brualla, T. Simon, J. Saragih, M. Nießner, R. Pandey, S. Fanello, G. Wetzstein, J.-Y. Zhu, C. Theobalt, M. Agrawala, E. Shechtman, D. B. Goldman, and M. Zollhöfer, “State of the Art on Neural Rendering,” *Computer Graphics Forum (EG STAR 2020)*, 2020.
- [26] Y. Xie, T. Takikawa, S. Saito, O. Litany, S. Yan, N. Khan, F. Tombari, J. Tompkin, V. Sitzmann, and S. Sridhar, “Neural fields in visual computing and beyond,” 2021. [Online]. Available: <https://neuralfIELDS.cs.brown.edu/>
- [27] R. T. Collins, “A space-sweep approach to true multi-image matching,” in *Proceedings CVPR IEEE Computer Society Conference on Computer Vision and Pattern Recognition*, 1996, pp. 358–363.
- [28] N. K. Kalantari, T.-C. Wang, and R. Ramamoorthi, “Learning-based view synthesis for light field cameras,” *ACM Trans. Graph.*, vol. 35, no. 6, Nov. 2016. [Online]. Available: <https://doi.org/10.1145/2980179.2980251>
- [29] I. Choi, O. Gallo, A. Troccoli, M. H. Kim, and J. Kautz, “Extreme view synthesis,” in *Proceedings of the IEEE International Conference on Computer Vision*, 2019, pp. 7781–7790.
- [30] P.-H. Huang, K. Matzen, J. Kopf, N. Ahuja, and J.-B. Huang, “Deepmvs: Learning multi-view stereopsis,” in *IEEE Conference on Computer Vision and Pattern Recognition (CVPR)*, 2018.
- [31] T. Zhou, R. Tucker, J. Flynn, G. Fyffe, and N. Snavely, “Stereo magnification: Learning view synthesis using multiplane images,” in *SIGGRAPH*, 2018.
- [32] P. P. Srinivasan, R. Tucker, J. T. Barron, R. Ramamoorthi, R. Ng, and N. Snavely, “Pushing the boundaries of view extrapolation with multiplane images,” in *2019 IEEE/CVF Conference on Computer Vision and Pattern Recognition (CVPR)*, 2019, pp. 175–184.
- [33] R. Tucker and N. Snavely, “Single-view view synthesis with multiplane images,” in *The IEEE Conference on Computer Vision and Pattern Recognition (CVPR)*, June 2020.
- [34] J. Flynn, M. Broxton, P. Debevec, M. DuVall, G. Fyffe, R. Overbeck, N. Snavely, and R. Tucker, “Deepview: View synthesis with learned gradient descent,” in *Proceedings of the IEEE Conference on Computer Vision and Pattern Recognition*, 2019, pp. 2367–2376.
- [35] T. Porter and T. Duff, “Compositing digital images,” in *Proceedings of the 11th Annual Conference on Computer Graphics and Interactive Techniques*, ser. SIGGRAPH ’84. New York, NY, USA: Association for Computing Machinery, 1984, p. 253–259. [Online]. Available: <https://doi.org/10.1145/800031.808606>
- [36] S. Lombardi, T. Simon, J. Saragih, G. Schwartz, A. Lehrmann, and Y. Sheikh, “Neural volumes: Learning dynamic renderable volumes from images,” *ACM Trans. Graph.*, vol. 38, no. 4, pp. 65:1–65:14, Jul. 2019.
- [37] O. Wiles, G. Gkioxari, R. Szeliski, and J. Johnson, “Synsin: End-to-end view synthesis from a single image,” in *Proceedings of the IEEE/CVF Conference on Computer Vision and Pattern Recognition*, 2020, pp. 7467–7477.
- [38] K.-A. Aliev, A. Sevastopolsky, M. Kolos, D. Ulyanov, and V. Lempitsky, “Neural point-based graphics,” in *Computer Vision – ECCV 2020*, A. Vedaldi, H. Bischof, T. Brox, and J.-M. Frahm, Eds. Cham: Springer International Publishing, 2020, pp. 696–712.
- [39] C. Lassner and M. Zollhöfer, “Pulsar: Efficient sphere-based neural rendering,” in *IEEE/CVF Conference on Computer Vision and Pattern Recognition (CVPR)*, June 2021.
- [40] G. Riegler and V. Koltun, “Stable view synthesis,” in *Proceedings of the IEEE Conference on Computer Vision and Pattern Recognition*, 2021.
- [41] S. Mehta and M. Rastegari, “Mobilevit: Light-weight, general-purpose, and mobile-friendly vision transformer,” in *International Conference on Learning Representations*, 2022. [Online]. Available: <https://openreview.net/forum?id=vh-0sUt8HIG>
- [42] I. Goodfellow, J. Pouget-Abadie, M. Mirza, B. Xu, D. Warde-Farley, S. Ozair, A. Courville, and Y. Bengio, “Generative adversarial nets,” in *Advances in Neural Information Processing Systems 27*, Z. Ghahramani, M. Welling, C. Cortes, N. D. Lawrence, and K. Q. Weinberger, Eds. Curran Associates, Inc., 2014, pp. 2672–2680. [Online]. Available: <http://papers.nips.cc/paper/5423-generative-adversarial-nets.pdf>
- [43] T.-Y. Lin, P. Dollár, R. Girshick, K. He, B. Hariharan, and S. Belongie, “Feature pyramid networks for object detection,” in *Proceedings of the IEEE conference on computer vision and pattern recognition*, 2017, pp. 2117–2125.
- [44] J. Reizenstein, R. Shapovalov, P. Henzler, L. Sbordone, P. Labatut, and D. Novotny, “Common objects in 3d: Large-scale learning and evaluation of real-life 3d category reconstruction,” in *International Conference on Computer Vision*, 2021.
- [45] A. Vaswani, N. Shazeer, N. Parmar, J. Uszkoreit, L. Jones, A. N. Gomez, L. U. Kaiser, and I. Polosukhin, “Attention is all you need,” in *Advances in Neural Information Processing Systems*, I. Guyon, U. V. Luxburg, S. Bengio, H. Wallach, R. Fergus, S. Vishwanathan, and R. Garnett, Eds., vol. 30. Curran Associates, Inc., 2017.
- [46] S. Peng, M. Niemeyer, L. Mescheder, M. Pollefeys, and A. Geiger, “Convolutional occupancy networks,” in *European Conference on Computer Vision*. Springer, 2020, pp. 523–540.
- [47] L. Chi, B. Jiang, and Y. Mu, “Fast fourier convolution,” in *Advances in Neural Information Processing Systems*, H. Larochelle, M. Ranzato, R. Hadsell, M. Balcan, and H. Lin, Eds., vol. 33. Curran Associates, Inc., 2020, pp. 4479–4488. [Online]. Available: <https://proceedings.neurips.cc/paper/2020/file/2fd5d41ec6cfab47e32164d5624269b1-Paper.pdf>
- [48] R. Suvorov, E. Logacheva, A. Mashikhin, A. Remizova, A. Ashukha, A. Silvestrov, N. Kong, H. Goka, K. Park, and V. Lempitsky, “Resolution-robust large mask inpainting with fourier convolutions,” in *Proceedings of the IEEE/CVF Winter Conference on Applications of Computer Vision*, 2022, pp. 2149–2159.
- [49] P. Nguyen, N. Sarafianos, C. Lassner, J. Heikkila, and T. Tung, “Human view synthesis using a single sparse rgb-d input,” 2021.
- [50] T. Müller, “Tiny CUDA neural network framework,” 2021, <https://github.com/nvlabs/tiny-cuda-nn>.
- [51] G. Riegler and V. Koltun, “Free view synthesis,” in *European Conference on Computer Vision*, 2020.
- [52] R. Zhang, P. Isola, A. A. Efros, E. Shechtman, and O. Wang, “The unreasonable effectiveness of deep features as a perceptual metric,” in *CVPR*, 2018.